Behavior of a Yawed Projectile for Thin Plate Penetration

DTIC QUALITY INSPECTED 2

S. Satapathy, A. Bedford, and S. Bless
Institute for Advanced Technology
The University of Texas at Austin

19970415 056

December 1996

IAT.R 0127

Approved for public release; distribution unlimited.

IAT Institute for Advanced Technology
The University of Texas at Austin

REPORT DOCUMENTATION PAGE

Form Approved
OMB NO. 0704-0188

1. AGENCY USE ONLY (Leave blank)	2. REPORT DATE	3. REPORT TYPE AND DATES COVERED
	December 1996	Technical report June - Dec. 1996

4. TITLE AND SUBTITLE

Behavior of a Yawed Projectile for Thin Plate Penetration

5. FUNDING NUMBERS

Contract # DAAA21-93-C-0101

6. AUTHOR(S)

S. Satapathy, A. Bedford, and S. Bless

7. PERFORMING ORGANIZATION NAME(S) AND ADDRESS(ES)

Institute for Advanced Technology
The University of Texas at Austin
4030-2 W. Braker Lane, #200
Austin, TX 78759

8. PERFORMING ORGANIZATION REPORT NUMBER

IAT.R 0127

9. SPONSORING / MONITORING AGENCY NAME(S) AND ADDRESS(ES)

U.S. Army Research Laboratory
ATTN: AMSRL-WT-T
Aberdeen Proving Ground, MD 21005-5066

10. SPONSORING / MONITORING AGENCY REPORT NUMBER

11. SUPPLEMENTARY NOTES

The view, opinions and/or findings contained in this report are those of the author(s) and should not be considered as an official Department of the Army position, policy, or decision, unless so designated by other documentation.

12a. DISTRIBUTION / AVAILABILITY STATEMENT	12b. DISTRIBUTION CODE
Approved for public release; distribution unlimited.	A

13. ABSTRACT *(Maximum 200 words)*

A long rod projectile is modeled as a free-free Timoshenko beam. While penetrating an oblique thin plate, the yawed projectile is subjected to a transverse point load traveling at a constant speed. The resulting equations are solved by applying Laplace transformation and numerical inversion. The effects of the slenderness ratio and the cross-section of the projectile on its transient behavior are studied.

14. SUBJECT TERMS

Long rod projectile, free-free Timoshenko beam, Laplace transformation, numerical inversion

15. NUMBER OF PAGES

28

16. PRICE CODE

17. SECURITY CLASSIFICATION OF REPORT	18. SECURITY CLASSIFICATION OF THIS PAGE	19. SECURITY CLASSIFICATION OF ABSTRACT	20. LIMITATION OF ABSTRACT
Unclassified	Unclassified	Unclassified	UL

Table of Contents

List of Figures

Behavior of a Yawed Projectile Penetrating a Thin Plate

Sikhanda Satapathy, Anthony Bedford and Stephan Bless

1.0 Introduction

In this paper we analyze the behavior of a yawed long rod projectile penetrating a plate. The plate is assumed to be thin enough that the effects of the axial forces exerted on the projectile during the initial impact and subsequent penetration can be neglected in comparison to the effects of the lateral force. As a result, the projectile is subjected to a lateral force which moves along its length at constant velocity as it engages the plate. The projectile is assumed to be sufficiently slender that it can be treated as a beam to model its dynamic behavior.

We therefore model the projectile's interaction with the plate as a beam subjected to a transverse point load traveling at constant speed. An extensive review of research on wave propagation in beams is given by Al-Mousawi [1]. The traditional Euler-Bernoulli beam theory is inadequate for analyzing the response of a beam to a moving load because high-frequency disturbances propagate at infinite velocity due to the infinite shear rigidity arising from neglect of shearing deformation [2]. We use Timoshenko beam theory, which takes into account shear deformation and rotatory inertia [3]. It predicts finite wave speeds at all frequencies and agrees very well with the dispersion relation for flexural waves obtained using the three dimensional Pochhammer-Chree theory [4].

Waves in beams have been analyzed through steady-state solutions obtained by superposition of normal modes [5] and by transform methods [6]. We apply the Laplace transform to analyze the transient response of a free-free Timoshenko beam subjected to a traveling point force and invert the transformed solution using a numerical technique [7]. Duffy [8] has compared the inversion technique we use with exact solutions for test cases involving poles and branch points.

2.0 Beam Equations

The equations governing flexural motion of a Timoshenko beam are given by:

$$EI\frac{\partial^2\psi}{\partial x^2} + k'AG\left[\frac{\partial y}{\partial x} - \psi\right] - \rho_p I\frac{\partial^2\psi}{\partial t^2} = 0 \qquad (1)$$

and

$$\rho_p A \frac{\partial^2 y}{\partial t^2} - k' AG\left[\frac{\partial^2 y}{\partial x^2} - \frac{\partial \psi}{\partial x}\right] = q(x,t) \ , \tag{2}$$

where E is Young's modulus, G is the shear modulus, ρ_p is the density, I is the moment of inertia, A is the cross-sectional area, k' is the Timoshenko shear coefficient which depends on the shape of the cross section, y is the transverse displacement, ψ is the rotation of the cross section due to moment alone, and q(x,t) is a distributed lateral force. The shear force, Q, and moment, M, are given by:

$$\frac{Q}{k'AG} = \frac{\partial y}{\partial x} - \psi = \frac{\partial y_1}{\partial x_1} - \psi \quad \text{and} \quad \frac{Mr}{EI} = r\frac{\partial \psi}{\partial x} = \frac{\partial \psi}{\partial x_1} \ . \tag{3}$$

The loading function q(x,t) is a Dirac delta function in the problem we consider. For a load moving with constant velocity V, q(x,t) can be written as:

$$q(x,t) = A_1 * \delta(x - Vt) \ , \tag{4}$$

where A_1 is a constant to be determined from the loading conditions. The governing equations can be nondimensionalized by introducing the change of variables:

$$t_1 = \frac{C_b t}{r}, \qquad x_1 = \frac{x}{r}, \quad \text{and} \quad y_1 = \frac{y}{r}, \tag{5}$$

where $C_b = \sqrt{E/\rho_p}$ is the bar wave speed and $r = \sqrt{I/A}$ is the radius of gyration. Using Eqs. (4) and (5), Eqs. (1) and (2) reduce to the following nondimensional forms:

$$\frac{\partial^2 \psi}{\partial x_1^2} + \frac{1}{\gamma}\left[\frac{\partial y_1}{\partial x_1} - \psi\right] - \frac{\partial^2 \psi}{\partial t_1^2} = 0 \tag{6}$$

and

$$\frac{\partial^2 y_1}{\partial t_1^2} - \frac{1}{\gamma}\left[\frac{\partial^2 y_1}{\partial x_1^2} - \frac{\partial \psi}{\partial x_1}\right] = \bar{A}\,\delta\left(x_1 - \frac{Vt_1}{C_p}\right), \qquad (7)$$

where $\gamma = E/(k'G)$ and $\bar{A} = \dfrac{A_1}{\rho_p A C_b^2}$.

Introducing the Laplace transforms:

$$Y(x_1, p) = \int_0^\infty y_1(x_1, t) e^{-pt}\, dt \quad \text{and} \quad \Psi(x_1, p) = \int_0^\infty \psi(x_1, t) e^{-pt}\, dt, \qquad (8)$$

Equations (6) and (7) transform to:

$$\Psi'' + \frac{1}{\gamma}[Y' - \Psi] - p^2\Psi = 0 \qquad (9)$$

and

$$p^2 Y - \frac{1}{\gamma}[Y'' - \Psi'] = \bar{A} e^{\frac{-x_1 C_b p}{V}}, \qquad (10)$$

where primes denote derivatives with respect to x_1. Boley and Chao [9] present the homogeneous solution of Equations (9) and (10) in the forms:

$$Y = C_1 e^{-\lambda_1 x_1} + C_2 e^{-\lambda_2 x_1} + C_3 e^{\lambda_1 x_1} + C_4 e^{\lambda_2 x_1} \qquad (11)$$

and

$$\Psi = \left(\frac{\lambda_1 - \gamma p^2}{\lambda_1}\right)\left(C_3 e^{\lambda_1 x_1} - C_1 e^{-\lambda_1 x_1}\right) + \left(\frac{\lambda_2 - \gamma p^2}{\lambda_2}\right)\left(C_4 e^{\lambda_2 x_1} - C_2 e^{-\lambda_2 x_1}\right), \qquad (12)$$

where:

$$\lambda_{1,2} = Bp^{1/2}\left[p \pm N\sqrt{p^2 - a^2}\right]^{1/2}, \;\; B = \sqrt{\frac{\gamma+1}{2}}, \;\; a = \frac{2}{\gamma-1}, \;\; \text{and} \;\; N = \frac{\gamma-1}{\gamma+1}. \quad (13)$$

The constants C_1, C_2, C_3 and C_4 will be determined from the boundary conditions. We must add particular solutions to Eqs. (11) and (12) corresponding to the forcing function given in Eq. (10). Eliminating ψ and its derivatives from Equations (9) and (10), we obtain:

$$Y'''' - Y''p^2(\gamma+1) + Yp^2(\gamma p^2+1) = \overline{A}\left[1+\gamma p^2 - \gamma\left(\frac{C_b p}{V}\right)^2\right]e^{\frac{-C_b p x_1}{V}}. \quad (14)$$

Assuming a particular solution of the form Y = C exp(-Dx_1), the constants C and D can be determined by substitution into Equation (14). The resulting general solution for Y is:

$$Y = C_1 e^{-\lambda_1 x_1} + C_2 e^{-\lambda_2 x_1} + C_3 e^{\lambda_1 x_1} + C_4 e^{\lambda_2 x_1} + \frac{\overline{A}\left[1+\gamma p^2 - \gamma\left(\frac{C_b p}{V}\right)^2\right]}{\left(\frac{C_b p}{V}\right)^4 - p^2(\gamma+1)\left(\frac{C_b p}{V}\right)^2 + p^2(\gamma p^2+1)} e^{\frac{-C_b p x_1}{V}}. \quad (15)$$

Similarly, eliminating Y and its derivatives from Equations (9) and (10), we obtain:

$$\Psi'''' - p^2(\gamma+1)\,\Psi'' + p^2(\gamma p^2+1)\,\Psi = -\overline{A}\,(C_b p/V)e^{-\frac{C_b p x_1}{V}}. \quad (16)$$

A general solution of this equation is:

$$\Psi = \left(\frac{\lambda_1 - \gamma p^2}{\lambda_1}\right)\left(C_3 e^{\lambda_1 x_1} - C_1 e^{-\lambda_1 x_1}\right) + \left(\frac{\lambda_2 - \gamma p^2}{\lambda_2}\right)\left(C_4 e^{\lambda_2 x_1} - C_2 e^{-\lambda_2 x_1}\right) + \frac{\overline{A}C_b p/V}{\left(\frac{C_b p}{V}\right)^4 - p^2(\gamma+1)\left(\frac{C_b p}{V}\right)^2 + p^2(\gamma p^2+1)} e^{-\frac{C_b p x_1}{V}}. \quad (17)$$

3.0 Boundary Conditions

The constants C_1, C_2, C_3 and C_4 in Equations (15) and (17) must be determined from the boundary conditions. For a free-free beam the end conditions are zero moment and zero shear force. From Eq. (3), the boundary conditions in terms of the dimensionless parameters of Eq. (5) are:

$$\frac{Q}{k'AG} = y_1' - \psi = 0 \text{ at } x = 0 \text{ and } x = L \tag{18}$$

and

$$\frac{Mr}{EI} = \psi' = 0 \text{ at } x = 0 \text{ and } x = L. \tag{19}$$

The Laplace transforms of these boundary conditions in terms of Eq. (8) are:

$$\left(Y' - \Psi\right)\Big|_{x_1=0,L/r} = \Psi'\Big|_{x_1=0,L/r} = 0\ . \tag{20}$$

Using the boundary conditions (20) together with Eqs. (15) and (17), the coefficients C_1, C_2, C_3 and C_4 can be expressed as:

$$\begin{bmatrix} -1 & -z_1 & 1 & z_1 \\ 1 & z_2 & 1 & z_2 \\ -z_3 & -z_1 z_4 & 1/z_3 & z_1/z_4 \\ z_3 & z_2 z_4 & 1/z_3 & z_2/z_4 \end{bmatrix} \begin{Bmatrix} C_1 \\ C_2 \\ C_3 \\ C_4 \end{Bmatrix} = -\begin{Bmatrix} \left(\lambda_1/\gamma p^2\right)\left(-F_1 C_b p/V + F_2\right) \\ \left(1/(\lambda_1^2 - \gamma p^2\right) C_b p F_2 / V \\ \left(\lambda_1 z_5/\gamma p^2\right)\left(-F_1 C_b p/V + F_2\right) \\ \left(z_5/(\lambda_1^2 - \gamma p^2\right) C_b p F_2 / V \end{Bmatrix}. \tag{21}$$

where $z_1 = \dfrac{\lambda_1}{\lambda_2}$; $z_2 = \dfrac{\lambda_2^2 - \gamma p^2}{\lambda_1^2 - \gamma p^2}$; $z_3 = e^{-(\lambda_1 L/r)}$; $z_4 = e^{-(\lambda_2 L/r)}$; $z_5 = e^{-\frac{\lambda_1 V}{C_b p}}$;

$$F_1 = \frac{\overline{A}\left[1 + \gamma p^2 - \gamma\left(\dfrac{C_b p}{V}\right)^2\right]}{\left(\dfrac{C_b p}{V}\right)^4 - p^2(\gamma + 1)\left(\dfrac{C_b p}{V}\right)^2 + p^2\left(\gamma p^2 + 1\right)} \text{ and}$$

$$F_2 = \frac{\bar{A} C_b p / V}{\left(\frac{C_b p}{V}\right)^4 - p^2(\gamma+1)\left(\frac{C_b p}{V}\right)^2 + p^2\left(\gamma p^2 + 1\right)}.$$

4.0 Estimation of the Lateral Force

The lateral force exerted on the projectile by the plate is estimated by determining the momentum flux of plate material displaced by the projectile. Consider a slender projectile of length L and radius of gyration r penetrating a thin plate of thickness h (Fig. 1) at velocity V_i. θ and ϕ are the yaw angle of the projectile and the angle of obliquity of the target, respectively. From the geometry of the impact, the speed at which the force travels along the length of the beam is:

$$V = V_i\left(\cos\theta + \frac{\sin\theta}{\tan\phi}\right) = V_i\frac{\sin(\theta+\phi)}{\sin(\phi)}. \tag{22}$$

Consider an element of the projectile of axial dimension dx passing through the target. If d is the span of target material intercepted by the projectile element dx, and the diameter of the projectile of circular cross-section (or the width of a projectile of rectangular cross section) is 2r, the momentum m, imparted to the projectile element dx in the transverse direction is given by:

$$m = 2\rho_t r h V_i \frac{\sin^2\theta}{\sin(\theta+\phi)} dx. \tag{23}$$

The time interval during which this momentum is encountered is:

$$\Delta t = \frac{dx}{V}. \tag{24}$$

Thus the force applied to the projectile, which is same as the constant in Equation (3), is:

$$A_l = 2\rho_t r h V_i^2 \frac{\sin^2\theta}{\sin\phi}. \tag{25}$$

The constant $\overline{A}$ in equation (7) becomes:

$$\overline{A} = 2\left(\frac{\rho_t}{\rho_p}\right)\left(\frac{r^2}{A}\right)\left(\frac{h}{r}\right)\left(\frac{V_i}{C_b}\right)^2 \frac{\sin^2\theta}{\sin\phi}. \tag{26}$$

Equation (26) takes into account only the momentum flux due to the inertia in estimating the lateral force. It is possible that the shearing force may play an important role in addition to the inertial forces under certain conditions. To investigate this, let us assume that the shearing force applied to the rod element dx varies linearly from F_s to zero during the time interval dt_s required to shear out the plate section. Then, the momentum, m_s imparted to the rod element, dx is $F_s * dt_s/2$. From the geometry of Figure 1, an expression for m_s can be derived as:

$$m_s = \frac{\sigma_0 h^2}{2V_i}\frac{\sin\theta}{\sin^2(\theta+\phi)}dx, \tag{27}$$

where σ_0 is the yield strength and hence, $\sigma_0/2$ is the shear strength of the plate material. The time interval during which this momentum is applied is same as the expression given in Eqn. (24). Thus from Eqns. (23) and (27) the ratio of the lateral forces arising out of inertia, A_1 and shear A_{1s} is:

$$\frac{A_{1s}}{A_1} = \frac{1}{4}\left(\frac{\sigma_0}{\rho_t V_i^2}\right)\left(\frac{h}{r}\right)\left(\frac{\sin\phi}{\sin\theta\ \sin^2(\theta+\phi)}\right). \tag{28}$$

For the case considered in the following section, the contribution of the shearing force is about 3% of the contribution due to the inertial force at an impact velocity of 2 km/s and hence can be ignored. However, at lower impact velocities or for thicker plates, shearing force gains importance and must be considered.

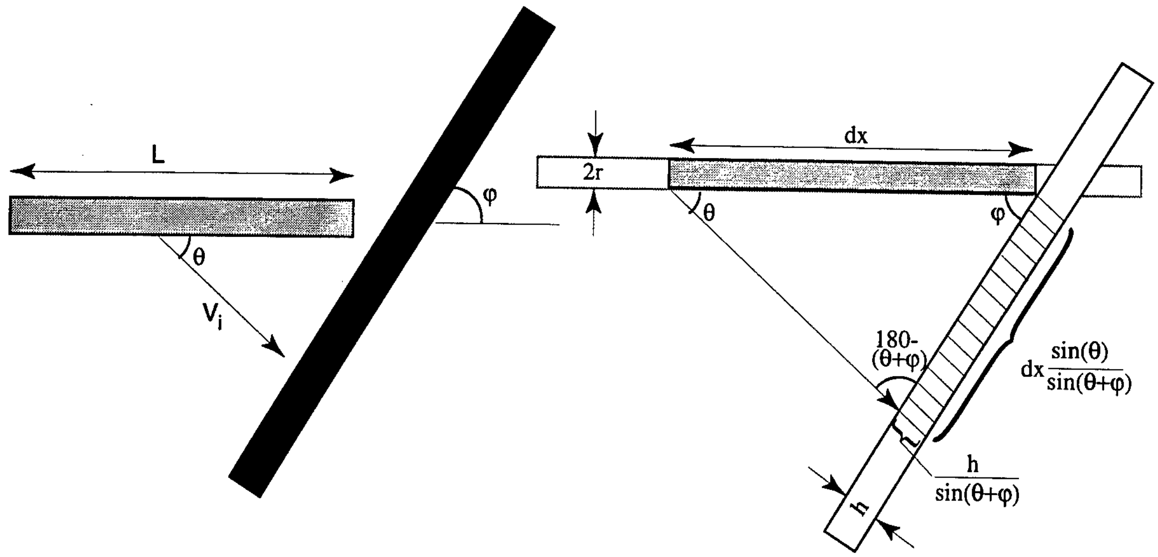

Figure 1. Geometry of impact.

5.0 Numerical Solution

To obtain time-dependent solutions for Y and Ψ, first Eq. (21) must be solved for the coefficients as functions of the Laplace variable p and then inverse Laplace transform must be applied to Eqs. (15) and (17). Closed-form solutions have been obtained for the case of a semi-infinite beam [6]. In this case the coefficient matrix in Eq. (21) is two-by-two, the coefficients can easily be expressed in terms of p, and with some effort, the transformed solutions can be inverted analytically to obtain the time-dependent solution. Closed-form solutions have also been obtained for finite beams with simpler boundary conditions [7].

Here we obtain a solution by numerically inverting Eqs. (15) and (17), which also requires numerical solution of Eq. (21) to obtain the values of the coefficients. Several methods are available for numerical inversion of Laplace transforms. Duffy [8] has compared the three most popularly used methods by estimating the deviations of the numerical solutions from exact solutions for various cases involving poles, branch points or both. He tested the methods using a closed-form solution obtained by Boley and Chao [10]. He observed that Crump's [9] method, without any correction for discretization error, yields very good agreement with the exact solution. We used the IMSL routine DINLAP [11] to invert our transforms, which uses a significantly improved Crump's method developed by de Hoog et al [12]. This method is based on applying the

epsilon algorithm to the complex Fourier series obtained as a discrete approximation to the inverse integral. We obtained the solutions by specifying an acceptable relative error of 1.E-4 or less. The IMSL routine DLSACG was employed to numerically solve Eq. (21). This routine solves the linear system of equations by LU decomposition followed by iterative refinement.

We considered a sample case of a long rod tungsten projectile penetrating a thin plate made of steel. The elastic constants used for tungsten are $E = 364$ GPa, $G = 140$ GPa, and $\rho_p = 17000$ kg/m^3. The target material was steel with a density of 7850 kg/m^3. The projectile was assumed to travel at 2 km/s with a 10° yaw angle. For a target obliquity of 85°, the velocity of the traveling load is also found to be 2 km/s from Eq. (25). In general, the impact velocity and the speed of the traveling load will be different, as evident from Eq. (25), depending upon the yaw angle and the angle of obliquity. The h/r ratio is taken as unity.

5.1 General Wave Structure and Effect of Aspect Ratio

The first set of calculations are for the transverse deflection y, shear force Q, and moment M at dimensionless times $t_1 = 10$, 20, 30 and 46 for a rod with aspect ratio, $L/r = 20$ and circular cross section ($k' = 1.1$). There are two distinct modes of wave propagation in a Timoshenko Beam with wave speeds of $C_b = \sqrt{(E/\rho_p)}$ and $C_s = \sqrt{(Gk'/\rho_p)}$. For tungsten, these speeds are 4627 m/s and 3010 m/s, respectively. The values $t_1 = 20$, 30 and 46 are the times at which the waves associated with C_b and C_s and the loading point arrive at the end of the beam. Figure 2 shows the distribution of the shear force in nondimensional form versus distance along the length of the projectile, normalized with respect to the radius of gyration. At dimensionless time $t_1 = 10$, these waves should be at $x_1 = 10$ and at $x_1 = 6.5$ respectively. In Fig. 2 a wave front exists at $x_1 = 10$ and the beam is undisturbed for $x_1 > 10$. At the second wave front, $x_1 = 6.5$, there is a distinct jump in the shear force. In addition, there exists a jump at $x_1 = 4.32$ which corresponds to the location of the force which travels at $V = 2$ km/s. The amplitude of the jump at the load can be determined analytically. At time t_1, the traveling load is at $x_1 = Vt_1/C_b$. Integrating Eq. (7) between $x_1 = Vt_1/C_b-\varepsilon$ and $x_1 = Vt_1/C_b+\varepsilon$, where ε is an arbitrarily small quantity, we obtain:

$$\frac{\partial^2}{\partial t_1^2}\int_{Vt_1/C_b-\varepsilon}^{Vt_1/C_b+\varepsilon} y_1 dx_1 - \frac{1}{\gamma}\left[\frac{\partial y_1}{\partial x_1}\Big|_{Vt_1/C_b-\varepsilon}^{Vt_1/C_b+\varepsilon} - \psi\Big|_{Vt_1/C_b-\varepsilon}^{Vt_1/C_b+\varepsilon}\right] = \overline{A}\int_{Vt_1/C_b-\varepsilon}^{Vt_1/C_b+\varepsilon}\delta(x_1 - Vt_1/C_b)dx_1 . \qquad (29)$$

The first integral in this equation is zero since y_1 is continuous. The second term is the jump in y_1', which is also zero because the slope of the beam is continuous. The third term expresses the jump in ψ at the load. From the definition of the delta function, the right-hand side is simply equal to $\overline{A}$. Thus, from Eqs. (7) and (29) we obtain a jump condition for shear as follows:

$$\left[\left|\frac{Q}{k'AG}\right|\right]_{x_1=Vt_1/C_b} = \left[\left|\frac{\partial y_1}{\partial x_1} - \psi\right|\right]_{x_1=Vt_1/C_b} = -[|\psi|]_{x_1=Vt_1/C_b} = -\gamma\overline{A}, \qquad (30)$$

where double brackets indicate a jump. For the above example, this jump is calculated to be 0.0038, which agrees with the value in Fig. 2. Given the nature of the numerical calculation, the agreement between the analytical value of the jump and the change in amplitude is excellent. The jump in shear force at the wave front associated with C_S has the same amplitude as the jump in shear force at the loading point since the wave originated at the loading point and propagates without dissipation. For $t_1 = 46$, the reflected wave front associated with C_S is calculated to be at the location $x_1 = 9.8$. Figure 2 shows a jump in shear force at this location for $t_1 = 46$, but it has the opposite sign compared to the jump in shear force at the loading point, as is expected of a wave reflected from a shear-free boundary.

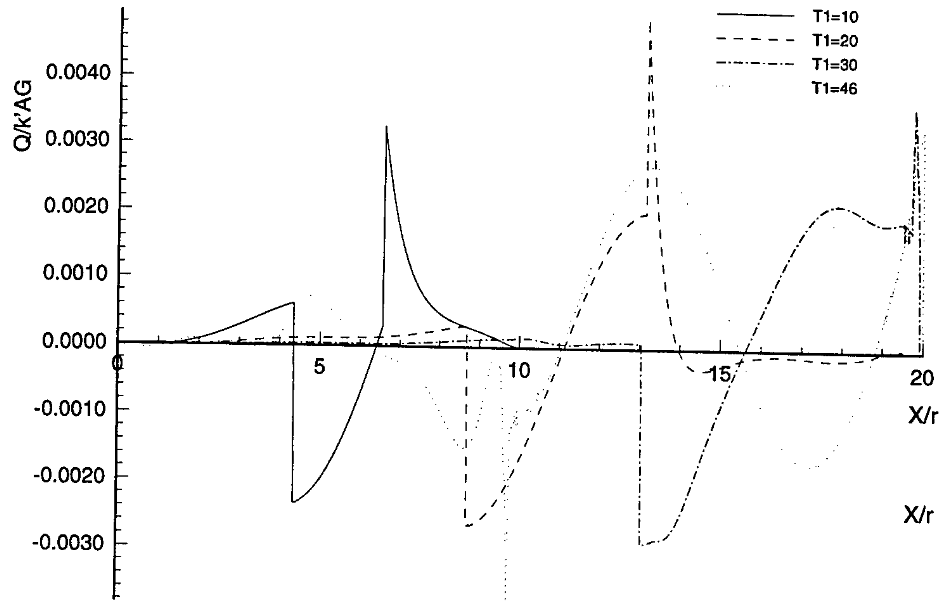

Figure 2. Shear distribution for L/r = 20 at different times.

Figure 3 shows the moment distribution in a beam with L/r = 20 for different times. The arrival time for the disturbance corresponds to the wave speed C_b. At the other wave fronts, associated with C_s and the point of load, the moment distribution shows peaks. But the maximum moment is not generally associated with these peaks; it occurs at the point where the shear force is zero. The maxima in shear force and moment do not occur simultaneously. In addition, there is no jump in moment anywhere, which is consistent with the jump condition associated with Eq. (10). The maximum moment in the beam is observed to occur at the time when the load is about to leave the beam and occurs at $x_1 \sim 15.5$. Figure 4 shows the deflection of the L/r = 20 beam at different times.

We also studied the effect of varying the ratio L/r on the wave propagation behavior. Figures 5, 6 and 7 show the distributions of shear force, moment and deflection for beams for L/r = 10, 20 and 30, respectively, at the time the load is about to exit the beams. k' was assumed to be 1.1, corresponding to a circular cross section. A larger L/r indicates either a larger length for the same stiffness or a smaller stiffness for the same length. The smaller the stiffness or larger the length, the larger is the maximum moment developed. The jumps in shear force are independent of L/r, as is expected from Eq. (30). However the maximum moment increases with L/r. This suggests that as the length of a projectile is increased, for a given load scenario, a point will be reached when failure occurs, and it will occur first at the uprange end of the projectile.

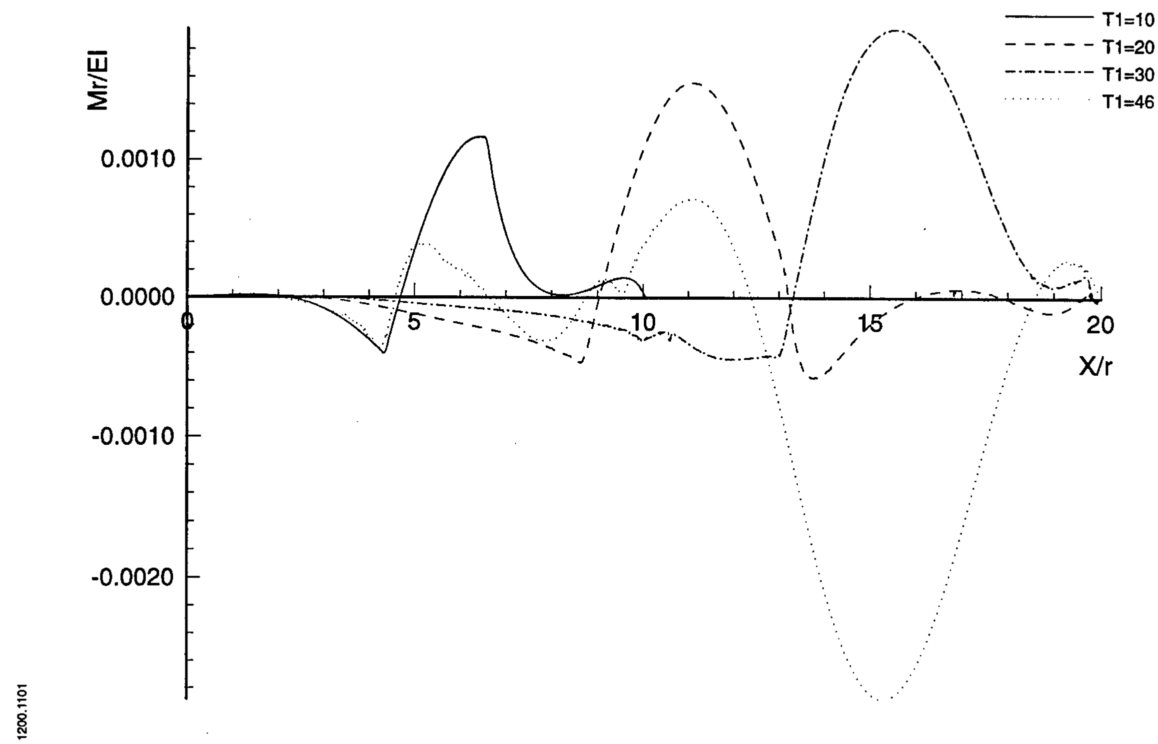

Figure 3. Moment distribution for L/r = 20 at different times.

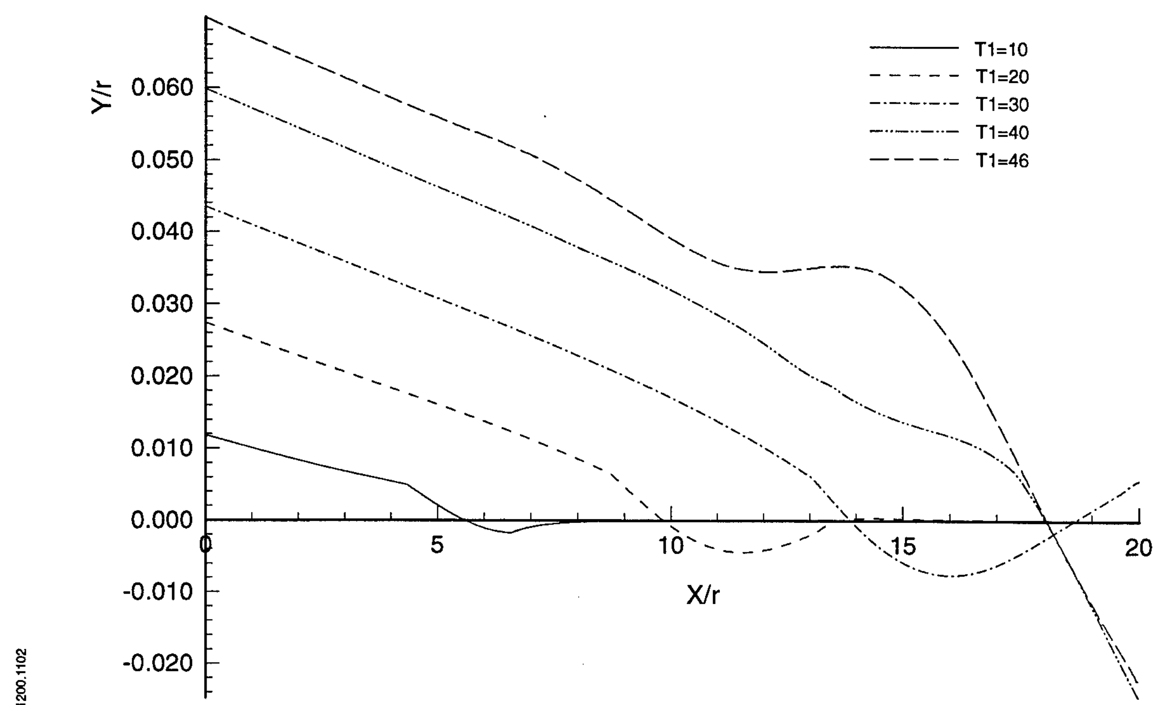

Figure 4. Deflection for L/r = 20 beam at different times.

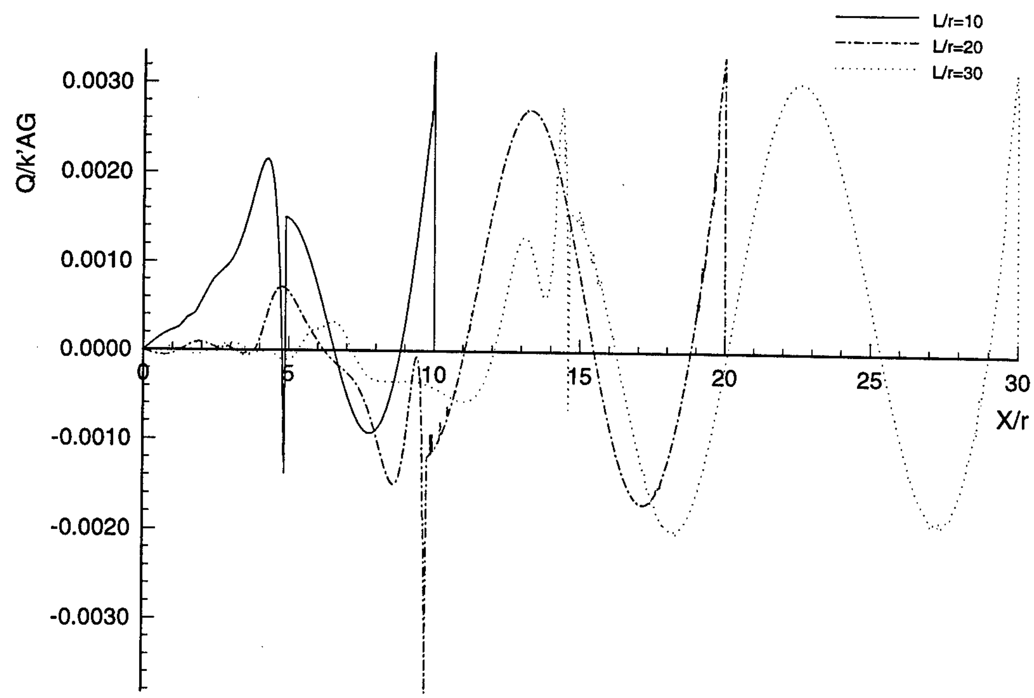

1200.1103

Figure 5. Shear distribution when the load exits the beam.

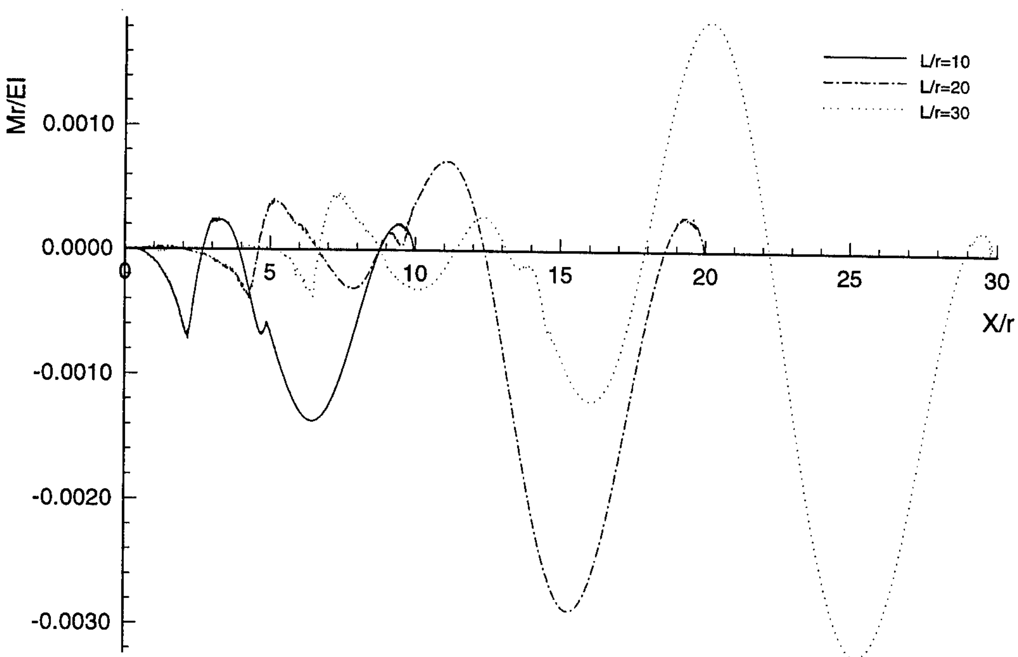

1200.1104

Figure 6. Moment distribution when the load exits the beam.

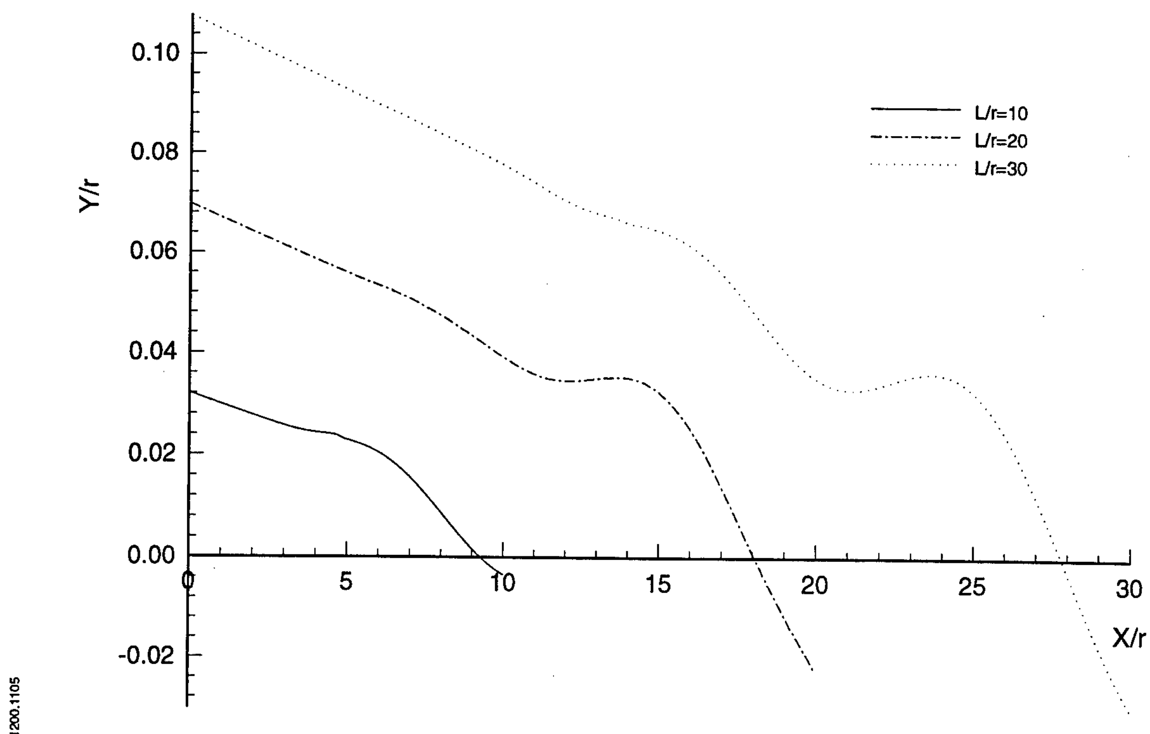

Figure 7. Deflection when the load exits the beam.

Finally, we checked to determine whether the beam material yielded in any of the cases noted above by employing the von Mises yield criteria. The yield criteria written in terms of the dimensionless quantities used above is:

$$\left[\left\{\left(\frac{Mr}{EI}\right)*E\right\}^2+3\left\{\left(\frac{Q}{k'AG}\right)*k'G\right\}^2\right]^{1/2}=\sigma_0\ , \qquad (31)$$

where σ_0 is the yield stress. From all our results, the maximum nondimensional shear experienced is below 0.005 (occurs for a L/r = 20 beam at $t_1 = 20$ and $x_1 = 13$), and the nondimensional moment at this point is about 0.0002. Inserting these values into Eq. (31) gives an effective stress value of 1.35 GPa, which is less than the yield stress of tungsten (about 1.5 GPa). Similarly, the maximum value of the nondimensional moment is about 0.003 (occurs for L/r = 20 at $t_1 = 46$ and $x_1 \sim 15$). The shear stress at this point is zero. Thus the maximum stress at this cross-section is 1.1 GPa, which is also below the yield stress value.

5.2 Effect of the Cross-Sectional Area

We compared the dynamic behavior of a projectile with circular cross-sectional area and a projectile with square cross sectional area, otherwise identical. In the following, we denote the quantities for square and circular cross-sectional area by subscripts "s" and "c" respectively. For the same cross-sectional area, the radii of gyration and the moments of inertia are related by:

$$\frac{r_s}{r_c} = \frac{1}{2}\sqrt{\frac{\pi}{3}}; \qquad \frac{I_s}{I_c} = \frac{\pi}{12}. \tag{32}$$

Thus from Eqs. (16) and (32) the nondimensional forcing functions for both the cases are related by:

$$\frac{\bar{A}_s}{\bar{A}_c} = \frac{r_s}{r_c} = \frac{1}{2}\sqrt{\frac{\pi}{3}}. \tag{33}$$

Since the beam equations are linear and we neglected the axial impulse, for a given beam the nondimensional quantity y_1, moment M, and shear force Q, should scale with the forcing function $\bar{A}$, i.e.:

$$\frac{y_{1s}}{y_{1c}} = \frac{(Mr/EI)_s}{(Mr/EI)_c} = \frac{(Q/k'AG)_s}{(Q/k'AG)_c} = \frac{\bar{A}_s}{\bar{A}_c}. \tag{34}$$

However, these quantities can not be compared in this fashion for beams with different cross section since the coefficients in the governing equation (e.g., Eq. (14)) will be different due to the fact that the numerical value of $\gamma = E/k'G$ changes with shape of the cross section. Changing k' will not only scale the jump in shear, as evident from Eq. (30), the wave speed of the second mode, C_s, will also scale with $\sqrt{k'}$. On the other hand, if we ignore the effect of k' and estimate only the effect of change in cross-sectional radius of gyration on the wave structures, from Eqs. (9), (32), (33) and (34) the following ratios of displacement, moment and shear for square and circular rods are obtained:

$$\frac{y_s}{y_c} = \frac{\bar{A}_s}{\bar{A}_c}\frac{r_s}{r_c} = \frac{\pi}{12}; \qquad \frac{M_s}{M_c} = \frac{I_s}{I_c}\frac{r_c}{r_s}\frac{\bar{A}_s}{\bar{A}_c} = \frac{\pi}{12}; \qquad \frac{Q_s}{Q_c} = \frac{k'_c}{k'_s}\frac{\bar{A}_s}{\bar{A}_c} = \frac{1.12}{0.9}\,\frac{1}{2}\sqrt{\frac{\pi}{3}} = 0.637. \qquad (35)$$

The nondimensional shear, moment and displacements are plotted in Figures 7, 8 and 9, respectively, for a square (k' = 0.9) and a circular rod (k' = 1.1) with L/r = 20 and identical material properties, at the time when the load exits the beams. The displacement scales almost identically to the ratio in Eq. (35), hence the effect of k' is minimal. Please note that necessary scaling constants have to be multiplied before comparing Eq. (35) with the nondimensional values in the figures. The shear jump scaled and shifted in accordance with the discussion above. The maximum value of the moment scaled almost in agreement with Eq. (35). Thus the deflection, maximum moment and maximum shear in the square rod are about 26%, 26% and 64% of those in the circular rod respectively. Consequently, square rods should fare better that circular rods as far as the bending vibration is concerned. Other, stiffer shapes should follow the same trend.

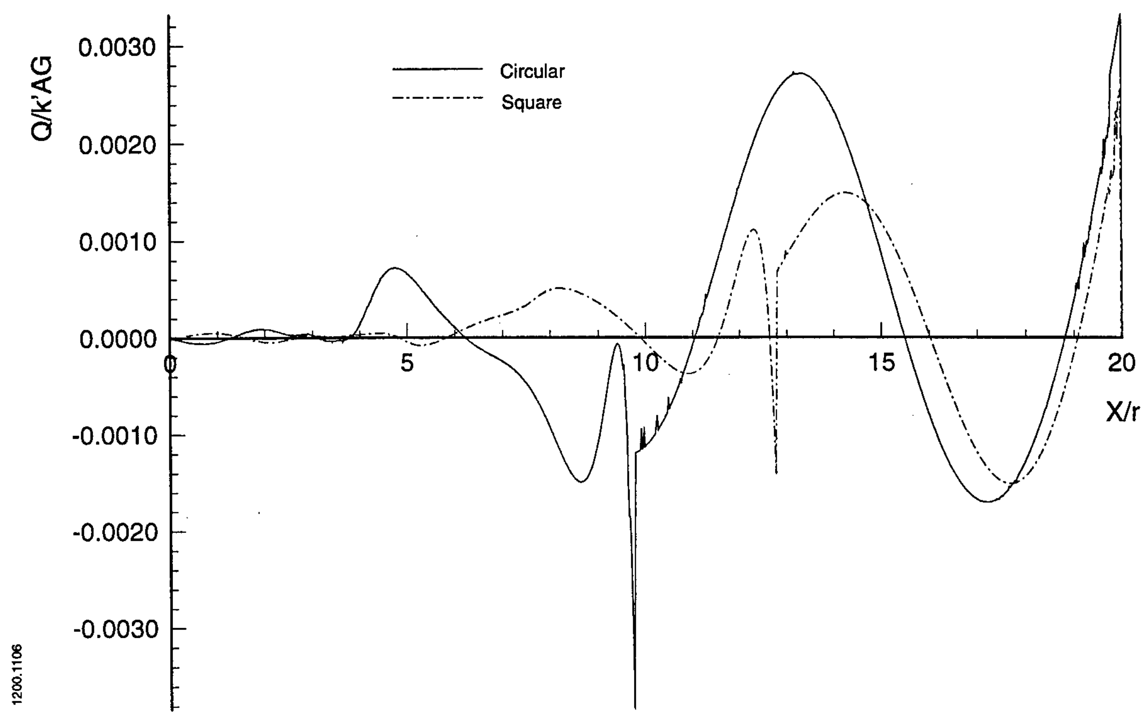

Figure 8. Shear distribution for square and circular beam.

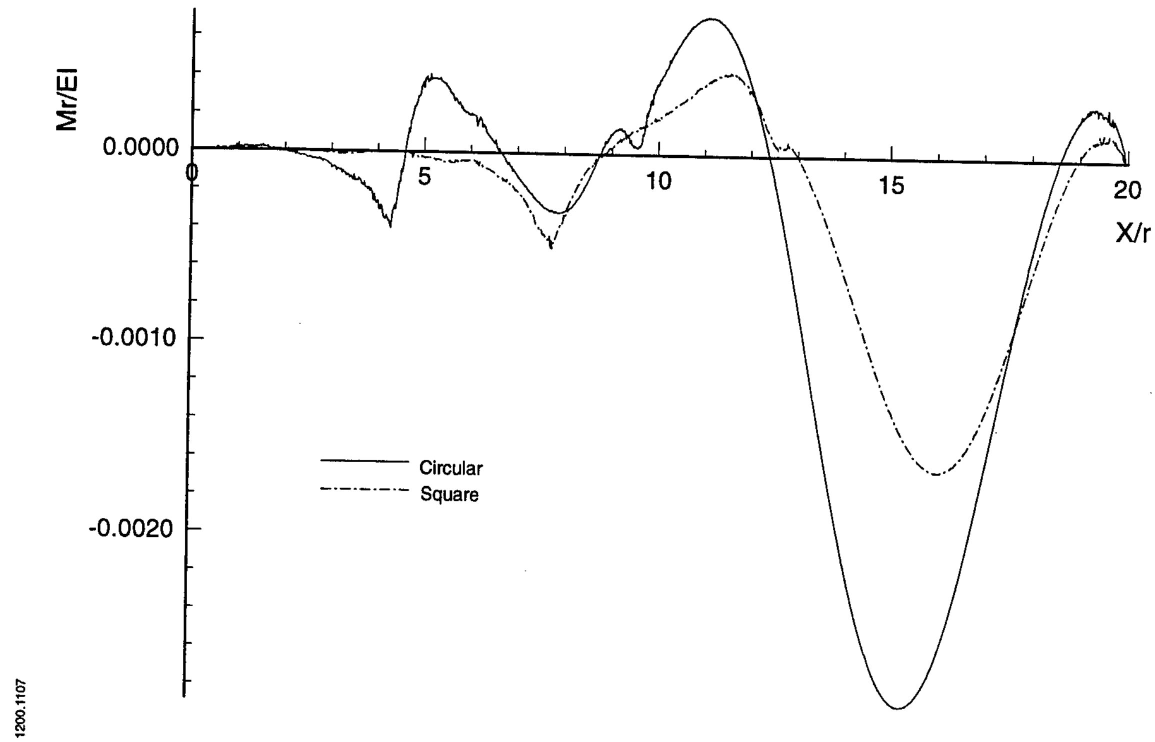

Figure 9. Moment distribution for square and circular beam.

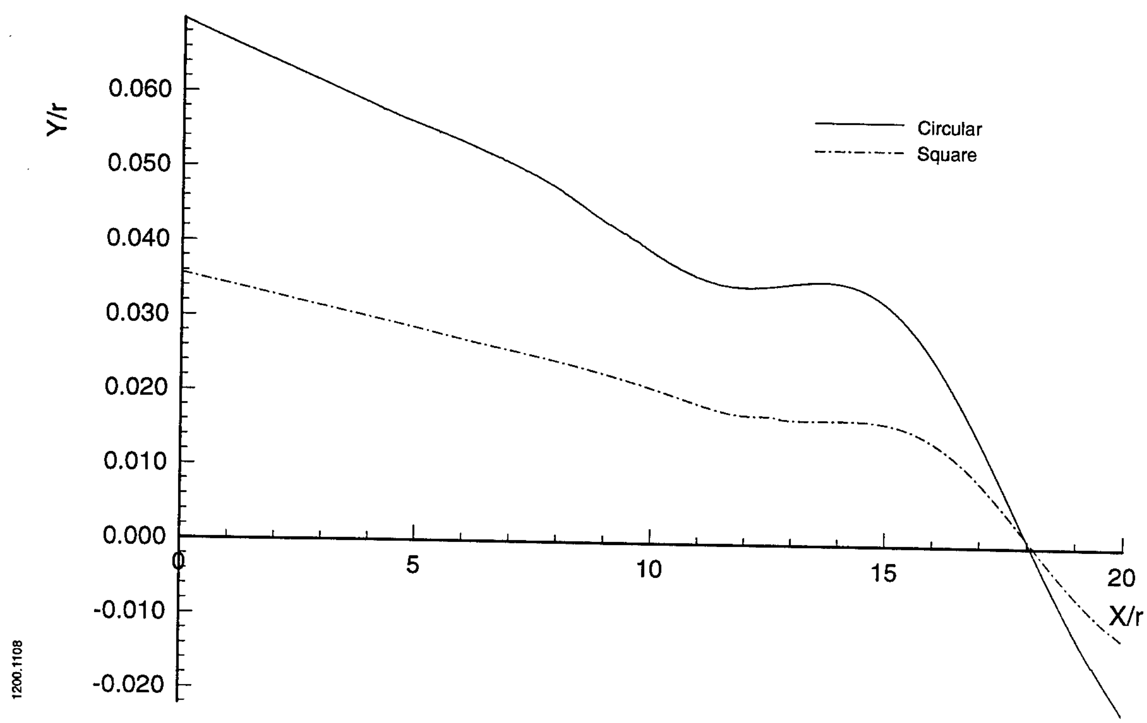

Figure 10. Deflection of square and circular beams when load exits the beam.

6.0 Conclusions

We have analyzed the transient response of a free-free Timoshenko beam subjected to a moving point load in order to understand the behavior of a yawed long rod projectile penetrating a thin oblique target. The Laplace transform technique with a numerical inversion method resulted in a well-resolved wave propagation solution which agreed well with theoretical wave speeds and jump conditions. We found that the maximum bending moment experienced increases with the projectile aspect ratio. Thus, in planning experiments or analyses, it is important to use projectiles that have appropriate L/r ratios. Moreover, the most likely failure location of a projectile is near the rear end, as failure is most likely to occur just after exit of the load. The bending stresses can be significantly reduced by changing the cross section; in general stiffer sections result in smaller stresses. This model can be used as a design tool to optimize the L/r ratio of the projectile for a given mass to ensure integrity of the projectile at high impact velocities. The elastic solutions obtained in the example were found to be adequate since the material does not yield at any time. For other angles of yaw and obliquity the maximum impact velocity of the projectile can be determined so that yielding does not take place anywhere in the projectile. For penetration of thicker plates, a solution can be constructed from the point load solution obtained in this paper by superposition principle as long as the axial impulse at impact is neglected. A plastic analysis would need to be undertaken if the behavior of the projectile must be determined under more severe loading conditions. Finally, an interesting extension to the present analysis would be to investigate the situation where the transverse load travels supersonically with respect to C_s or C_b.

Acknowledgment

This work was supported by the U. S. Army Research Laboratory (ARL) under contract DAAA21-93-C-0101.

References

[1] Al-Mousawi, M. M., "Theoretical Studies on Flexural Wave Propagation in Beams: A Comprehensive Review - Part I: Historical Background," *Shock and Vibration Digest*, vol. 18, no. 4, p. 11, 1986.

[2] Graff, K. E., *Wave Motion in Elastic Solids*, Dover Publications, New York, 1975.

[3] Weaver, W., Timoshenko, S. P., and Young, D. H., *Vibration Problems in Engineering*, John Wiley and Sons, New York, 1990.

[4] Kolsky, H., *Stress Waves in Solids*, Dover Publications, New York, 1963.

[5] Anderson, R. A., "Flexural Vibrations in Uniform Beams According to the Timoshenko Theory," *Trans. ASME*, vol. 75, p. 504, 1953.

[6] Florence, A. L., "Traveling Force on a Timoshenko Beam," *J. Appl. Mech.*, vol. 32, no. 2, p. 351, 1965.

[7] Miklowitz, J., "Flexural Wave Solutions of Coupled Equations Representing the More Exact Theory of Bending," *Trans. ASME*, vol. 75, p. 511, 1953.

[8] Duffy, D. G., "On the Numerical Inversion of Laplace Transforms: Comparison of Three New Methods on Characteristic Problems from Applications," *ACM Transactions on Mathematical Software*, vol. 19, no. 3, p. 333, 1993.

[9] Crump, K. S., "Numerical Inversion of Laplace Transforms Using a Fourier Series Approximation," *J. ACM*, vol. 23, no. 1, p. 89, 1976.

[10] Boley, B. A. and Chao, C. C., "Some Solutions of the Timoshenko Beam Equations," *J. Appl. Mech.*, vol. 77, p. 579, 1955.

[11] IMSL, "INLAP - Compute the Inverse Laplace Transform," *IMSL Math/Library* Version 1.1., pp. 756-758, January 1989.

[12] de Hoog, F. R., Knight, J. H. and Stokes, A. N., "An Improved Method for Numerical Inversion of Laplace Transforms," *SIAM Journal on Scientific and Statistical Computing*, vol. 3, pp. 357-366, 1982.

Distribution List

Administrator
Defense Technical Information Center
Attn: DTIC-DDA
8725 John J. Kingman Road, Ste 0944
Ft. Belvoir, VA 22060-6218

Director
US Army Research Lab
ATTN: AMSRL OP SD TA
2800 Powder Mill Road
Adelphi, MD 20783-1145

Director
US Army Research Lab
ATTN: AMSRL OP SD TL
2800 Powder Mill Road
Adelphi, MD 20783-1145

Director
US Army Research Lab
ATTN: AMSRL OP SD TP
2800 Powder Mill Road
Adelphi, MD 20783-1145

Army Research Laboratory
AMSRL-CI-LP
Technical Library 305
Aberdeen Prvg Grd, MD 21005-5066

Dr. Charles Anderson, Jr.
Southwest Research Institute
Engineering Dynamics Department
P.O. Box 28510
San Antonio, TX 78228-0510

Dr. Anthony Bedford
Aerospace Engineering Dept.
University of Texas at Austin
Austin, TX 78705

Todd Bjerke
Director
U.S. Army Research Laboratory
Attn: AMSRL-WT-TC
Aberdeen Prvg Grd, MD 21005-5066

N. Singh Brar
University of Dayton Research Institute
300 College Park
Shroyer Park Center
Dayton, OH 45469-0182

Randolph S. Coates
US Army Research Laboratory
AMSRL-WT-TC
APG, MD 21005-5066

William deRosset
U.S. Army Research Laboratory
Attn: AMSRL-WT-TC
Aberdeen Prvg Grd, MD 21005-5066

Timothy G. Farrand
U.S. Army Research Laboratory
ATTN: AMSRL-WT-TD
Aberdeen Prvg Grd, MD 21005-5066

Dr. Michael Forrestal
Sandia National Laboratory
Division 1922
P.O. Box 5800
Albuquerque, NM 87185

Dr. Joe Foster
Air Force Armament & Technology Lab
AFATL/MNW
Eglin AFB, FL 32542

Konrad Frank
U.S. Army Research Laboratory
Attn: AMSRL-WT-TD
Aberdeen Prvg Grd, MD 21005-5066

Mr. Tom Furmaniak
TACOM
U.S. Army Tank and Auto Command
AMSTA-JSK
Warren, MI 48397-5000

Dr. W. J. Gillich
U.S. Army Research Laboratory
AMSRL-WT-TA
Aberdeen Prvg Grd, MD 21005-5066

Tim Holmquist
Alliant Techsystems, Inc.
Twin City Army Ammunition Plant-Bldg. 103
New Brighton, MN 55112

Kailasam Iyer
US Army Research Office
P.O. Box 1221
Research Triangle Park, NC 27709-2211

Richard Lloyd
Raytheon
Mail Stop T3TB8
P.O. Box 1201
Tewksburg, MA 01876-0901

Nick Lynch
DERA Fort Halstead
Bldg. A 20, Div. WX5
Sevenoaks, Kent
England TN14 7BP

Distribution List

Mr. Dennis L. Orphal
International Research Associates
4450 Black Ave. Suite E
Pleasanton, CA 94566

Martin N. Raftenberg
US Army Research Lab
AMSRL-WT-TD
Aberdeen Prvg Grd, MD 21005-5066

Daniel R. Scheffler
U.S. Army Research Laboratory
ATTN: AMSRL-WT-TC
Aberdeen Prvg Grd, MD 21005-5066

Edward Schmidt
U.S. Army Research Laboratory
Attn: AMSRL-WT-PB
Aberdeen Prvg Grd, MD 21005-5066

Graham Silsby
U.S. Army Research Laboratory
Aberdeen PG, MD 21005

Jerome D. Yatteau
Applied Reseach Associates
5941 South Middlefield Rd, Suite 100
Littleton, Colorado 80123